Available online at www.sciencedirect.com
SCIENCE DIRECT®
Journal of Solid State Chemistry 178 (2005) 1386–1394
JOURNAL OF SOLID STATE CHEMISTRY
www.elsevier.com/locate/jssc

# Inorganic–organic hybrid polyoxometalate: Preparation, characterization and electrochemistry properties

Zhangang Han, Yulong Zhao, Jun Peng*, Aixiang Tian, Yuhua Feng, Qun Liu

*Faculty of Chemistry, Northeast Normal University, No. 138 Renmin Street, Changchun City, Jilin province, 130024, PR China*

Received 29 November 2004; received in revised form 1 February 2005; accepted 7 February 2005
Available online 14 March 2005

**Abstract**

The solid hybrid material $(H_{3/4}pbpy)_4[PMo_{12}O_{40}]\cdot 1.25H_2O$ (**1**) (pbpy = 5-phenyl-2-(4-pyridinyl)pyridine) has been prepared and characterized. A structural feature of compound **1** is that the polyoxometalate anions exhibit a one-dimensional inorganic double chain-like structure via weak interactions of O…O. The organic moiety exhibits regular packing with offset aromatic–aromatic interactions between the pbpys, leading to a compact supramolecular framework structure to accommodate the inorganic chains. Compound **1** was employed to fabricate the three-dimensional bulk-modified carbon paste electrode (**1**-CPE) to research on its electrochemistry properties. The results indicate that **1** retained Keggin molybdate anion electrocatalytic activities toward the reduction of chlorate, hydrogen peroxide and nitrite.


*Keywords:* Inorganic–organic hybrid; Polyoxometalate; Electrochemistry; Carbon paste electrode; Electrocatalysis

## 1. Introduction

In the past few years, a significant attention continues to focus on polyoxometalates (POMs) on account of their intriguing architectures and potential applications in many research fields [1]. As one kind of metal oxide clusters with nanosizes and abundant topologies, POMs have been employed as inorganic building blocks for the construction of supramolecular arrays with various organic ligands due to their ability to accept electrons. They can be combined with organic π-electron donors, such as N-containing ligands, amino acids, polypeptides, organometallics, tetrathiafulvalene (TTF), bis (ethylenedithio)tetrathiafulvalene (ET) and perylene (per), to form POM-based hybrid materials [2–6]. Many studies have also shown that this kind of hybrid materials possesses some active physical properties, such as electrical, magnetic, and optical properties which are associated with structures constructed by so-called anion–cation salts or host-guest solids.

POMs with the ability to undergo reversible multi-electron redox process are good candidates for chemically modified electrode (CME) [7]. The traditional CME with POMs can be achieved by the following methods: (i) surface modification, including electrodeposition, adsorption, doping into polymer matrices, self-assembly, layer-by-layer deposition and LB methods [8]; (ii) sol–gel film-modified electrode [9] and (iii) other strategies [10]. However, a drawback in the application of the conventional POMs is their poor long-term stability due to good solubility [11]. Recently, a research interest has been focused on the design and preparation of novel POM-based hybrid materials, as well as the application of them in three-dimensional bulk-modified carbon paste electrode (CPE) by direct mixing [12]. Chemically bulk-modified CPE is a mixture of a modifier, graphite powder and paste liquid, which has been widely applied in electrochemistry with advantages: inexpensive, easy to handle and prepare [13]. In general, the modifiers used by direct mixing should be

*Corresponding author. Fax: +86 431 5684009.
*E-mail address:* jpeng@nenu.edu.cn (J. Peng).

0022-4596/$ - see front matter © 2005 Elsevier Inc. All rights reserved.
doi:10.1016/j.jssc.2005.02.006

insoluble in the analytic solution, as well as should be absorbed strongly by carbon paste in order to avoid dissolution of the molecules from the electrode surface during the measurements. Therefore, traditional POMs cannot be directly used as a bulk modifier of CPE owing to their good solubility. Inorganic–organic hybrids of POMs prepared by hydrothermal reaction are of usually poor solubility in water and in common organic solvent, whose property is very advantageous to expand POM-based materials' application in chemically bulk-modified electrode.

Organic molecule 5-phenyl-2-(4-pyridinyl) pyridine (pbpy) with tricycles, aromatic entity has a straight and planar structure with an extended π-electron conjugated system. In current research work, we chose the electron-rich pbpy as organic moiety to prepare POM-based hybrid. Herein, the synthesis, crystal structure and electrochemical property of a new inorganic–organic POM hybrid, $(H_{3/4}pbpy)_4[PMo_{12}O_{40}]\cdot 1.25H_2O$ (**1**), were reported. Compound **1** was employed to fabricate the three-dimensional bulk-modified carbon paste electrode (**1**-CPE) to research on its electrochemistry and electrocatalytic properties toward the reduction of chlorate, hydrogen peroxide and nitrite.

## 2. Experimental section

### 2.1. General methods

All chemicals purchased were of reagent grade and used without further purification. Organic molecule pbpy was synthesized in laboratory and confirmed by $^1$H NMR and IR. Elemental analyses (C, H and N) were performed on a Perkin–Elmer 2400 CHN elemental analyzer. IR spectra were recorded in the range 400–4000 $cm^{-1}$ on an Alpha Centaurt FT/IR spectrophotometer using KBr pellets. UV spectra were measured on a Shimadzu UV 3100 spectrophotometer. Cyclic voltammograms (CV) were recorded on a 384B polarographic analyzer. A CHI 660 Electrochemical Workstation connected to a Digital-586 personal computer was used for control of the electrochemical measurements and for data collection. A conventional three-electrode system was used. The working electrode was a modified CPE. An Ag/AgCl (saturated KCl) electrode was used as a reference electrode and a Pt gauze as a counter electrode. All potentials were measured and reported versus the Ag/AgCl electrode.

### 2.2. Hydrothermal synthesis

$(H_{3/4}pbpy)_4[PMo_{12}O_{40}]\cdot 1.25H_2O$ (**1**) was synthesized from the reaction mixture of $Na_2MoO_4\cdot 2H_2O$ (2.5 mmol), $H_3PO_4$ (ca. 1.0 mmol), pbpy (0.2 mmol) and $H_2O$ (10 mL) in an 18 mL Teflon-lined reactor under autogenous pressure at 165 °C for 4 days, followed by slowly cooling (10 °C/h) to room temperature. Black block crystals were obtained, washed with distilled water and air-dried. Elemental Anal. Found: C, 27.68; H, 1.93; N, 4.04%. Calcd. For $C_{64}H_{53.5}Mo_{12}N_8O_{41.25}P$: C, 27.64; H, 1.96; N, 3.99%.

### 2.3. Preparation of compound *1* modified CPE (*1*-CPE)

Compound **1** modified CPE (**1**-CPE) was fabricated as follows: 0.5 g graphite powder and 0.05 g compound **1** were mixed, and ground together by an agate mortar and pestle to achieve an even, dry mixture; to the mixture 0.50 mL paraffin oil was added and stirred with a glass rod; then the mixture was used to pack into 3 mm inner diameter glass tube, and the surface was pressed tightly onto weighing paper with a copper rod through the back. Electrical contact was established with a copper rod through the back of the electrode.

### 2.4. X-ray crystallographic study

Single crystal of **1** with dimension $0.160\times 0.140\times 0.130$ mm was glued on a glass fiber. Data were collected on a Rigaku R-AXIS RAPID IP diffractometer with Mo$K\alpha$ monochromatic radiation ($\lambda = 0.71703$ Å) at 293 K. Empirical absorption correction was applied. The structurec was refined by the full-matrix least-squares method on $F^2$ using the SHELXTL crystallographic software package [14]. Anisotropic thermal parameters were used to refine all non-hydrogen atoms. The protonized H(1B), H(3B), and half-occupied H(2B) atoms were located from different Fourier maps. Half-occupied H(4B) and other hydrogen atoms were located in the idealized positions. Crystal data were listed in Table 1.

CCDC-256357 contains the supplementary crystallographic data for this paper. These data can be obtained free of charge at www.ccdc.cam.ac.uk/conts/retrieving.html [or from the Cambridge Crystallographic Data Center, 12 Union Road, Cambridge CB2 1EZ, UK; Fax: (internet.) +44-1223/336-033; E-mail: deposit@ccdc.cam.ac.uk].

## 3. Results and discussion

### 3.1. Crystal structure

The crystal structure analysis reveals that compound **1** consists of one $PMo_{12}O_{40}^{3-}$ anion, four pbpys, and one and a quarter water molecules (see Fig. 1). As shown in Fig. 1, the anion shows a classical 'α-Keggin' structure [15]. The tetrahedron-coordinated P is surrounded by four oxygen atoms with P–O bonds ranging from

Table 1
Crystal data and structure refinement for **1**

| | |
|---|---|
| Empirical formula | C64 H53.5 Mo12 N8 O41.25 P1 |
| Formula weight | 2774.54 |
| Temperature | 293(2) K |
| Wavelength | 0.71073 Å |
| Crystal system, space group | Monoclinic, $P2(1)/c$ |
| Unit cell dimensions | $a = 19.778(4)$ Å $\alpha = 90°$ |
| Volume | $b = 13.046(3)$ Å $\beta = 98.07(3)°$ |
| $Z$, Calculated density | $c = 31.575(6)$ Å $\gamma = 90°$ |
| Absorption coefficient | 8066(3) Å$^3$ |
| $F(000)$ | 4, 2.285 Mg/m$^3$ |
| Crystal size | 1.918 mm$^{-1}$ |
| $\theta$ range for data collection | 5360 |
| Limiting indices | 0.160 × 0.140 × 0.130 mm |
| Reflections collected/unique | 3.04–27.48° |
| Completeness to $\theta = 27.48$ | $-25 \leqslant h \leqslant 25$, $-16 \leqslant k \leqslant 16$, $-40 \leqslant l \leqslant 40$ |
| Absorption correction | 71399/18369 [$R$(int) = 0.0517] |
| Max. and min. transmission | 99.30% |
| Refinement method | Empirical |
| Data/restraints/parameters | 0.779 and 0.742 |
| Goodness-of-fit on $F^2$ | Full-matrix least-squares on $F^2$ |
| Final $R$ indices [$I > 2\sigma(I)$] | 18369/0/1175 |
| $R$ indices (all data) | 1.052 |
| Extinction coefficient | $R1 = 0.0409$, w$R2 = 0.0909$ |
| Largest diff. peak and hole | $R1 = 0.0556$, w$R2 = 0.0942$ |
| | 0.00024(2) |
| | 0.937 and −0.869 e. Å$^{-3}$ |

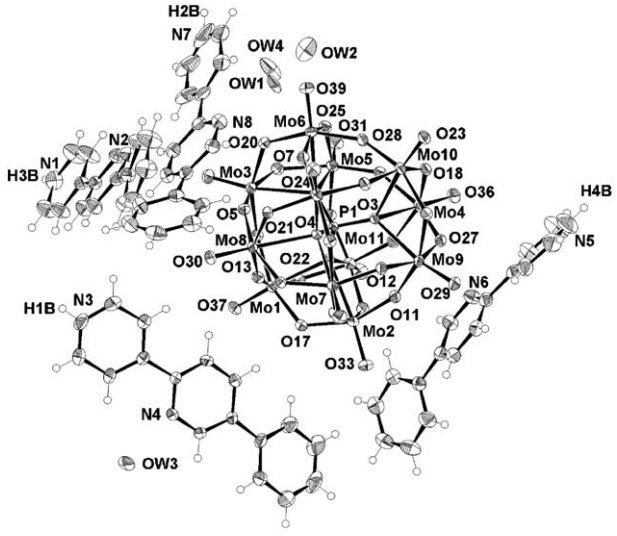


Fig. 1. ORTEP drawing of **1** showing the labeling of atoms with thermal ellipsoids at 35% probability.

1.525(3) to 1.534(3) Å (mean 1.529 Å). The Mo–O distances vary over a wide range 1.666–2.470 Å. The shortest Mo–O distances for the unshared oxygen atoms are in the range of 1.666–1.686 Å (mean value, 1.678 Å); the longest Mo–O distances involving O atoms of the central tetrahedron are in the range of 2.408–2.470 Å (mean value, 2.440 Å); the Mo–O distances for the bridging oxygen atoms vary from 1.832 to 2.017 Å (mean value, 1.918 Å). These results show that the $PO_4$ tetrahedron and $MoO_6$ octahedra of the anion are severely distorted, and may be ascribed to the strong interaction between the polyanions and organic moiety. A striking structural feature is that the anions extend the linkage into a one-dimensional inorganic double chain-like structure via weak interactions: O(40)…O(38) 2.960 Å, O(23)…O(16) 2.931 Å and O(23)…O(18) 3.001 Å along the direction of $b$-axis (see Fig. 2).

The organic moiety exhibits regular packing with face-to-face aromatic–aromatic interactions between the pbpys, leading to a compact supramolecular framework structure to accommodate one-dimensional inorganic chains (Fig. 3). In the structure of **1**, the four crystallographically distinct pbpy molecules are labeled as: N(1)-pbpy, N(3)-pbpy, N(5)-pbpy and N(7)-pbpy. Multiple hydrogen bonds exist between the closely approached clusters, water molecules and organic moiety (see Table 2). The hydrogen bonding distances between N(3) atom of pbpy and oxygen atoms of $PMo_{12}O_{40}^{3-}$ anion are N(3)…O(8): 2.889 Å, N(3)…O(10): 3.000 Å, N(3)…O(22): 2.905 Å and N(3)…O(24): 3.036 Å.The N(1)-pbpy lies on the opposite side of $PMo_{12}O_{40}^{3-}$, the hydrogen bonding distances are 2.881, 2.991, 3.160 and 3.325 Å for N(1)…O(12), N(1)…O(16), N(1)…O(35) and N(1)…O(6), respectively. Thus, an interesting organic bicapped-Keggin (Fig. 4) structure is presented if these weak interactions are taken into account, which we have reported recently [16]. In addition, N(5)- and N(7)-containing pbpys have hydrogen bonding distances of N(5)…O(38) = 2.947 Å and N(7)…O(24) = 2.698 Å with the anion, respectively. In contrast to N(1)- and N(3)-containing pbpy molecules, the N(5)- and N(7)-containing pbpys are strongly distorted. The dihedral angles between the planes of phenyl-rings and adjacent pyridine planes are ca.17.51°, 8.83°, 39.84° and 37.66° for N(1)-, N(3)-, N(5)- and N(7)-containing pbpy molecules, respectively. The severe distortions further indicate that the strong interactions between inorganic and organic units. There are offset face-to-face $\pi-\pi$ interactions between adjacent pbpys: the N(1)- and N(3)-containing pbpys are almost parallel to each other, while N(5)- and N(7)-containing pbpys have near 45° angle with N(1)-containing pbpy along different directions. Four types of crystallographically distinct pbpy molecules arrange compactly to lead to the formation of channels where the guest $PMo_{12}O_{40}^{3-}$ chains are located (Fig. 5).

### 3.2. Spectroscopic characterization

In the IR spectrum, there are four characteristic asymmetric vibrations resulting from Keggin polyanion.

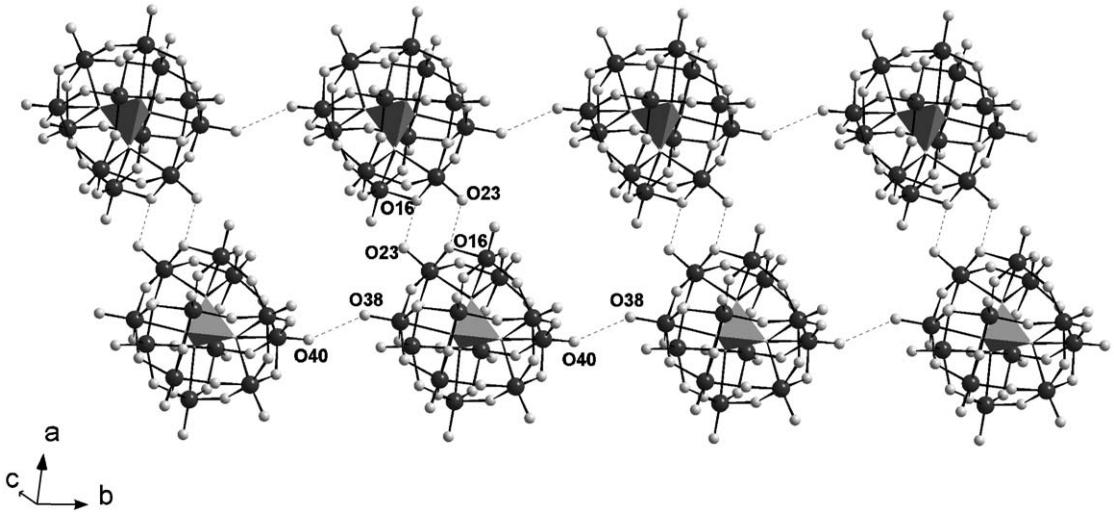


Fig. 2. A representation of the one-dimensional double chain running parallel to the crystallographic *b* axis (polyhedra, $PO_4$ tetrahedron). Organic pbpys and water molecules are omitted for clarity.

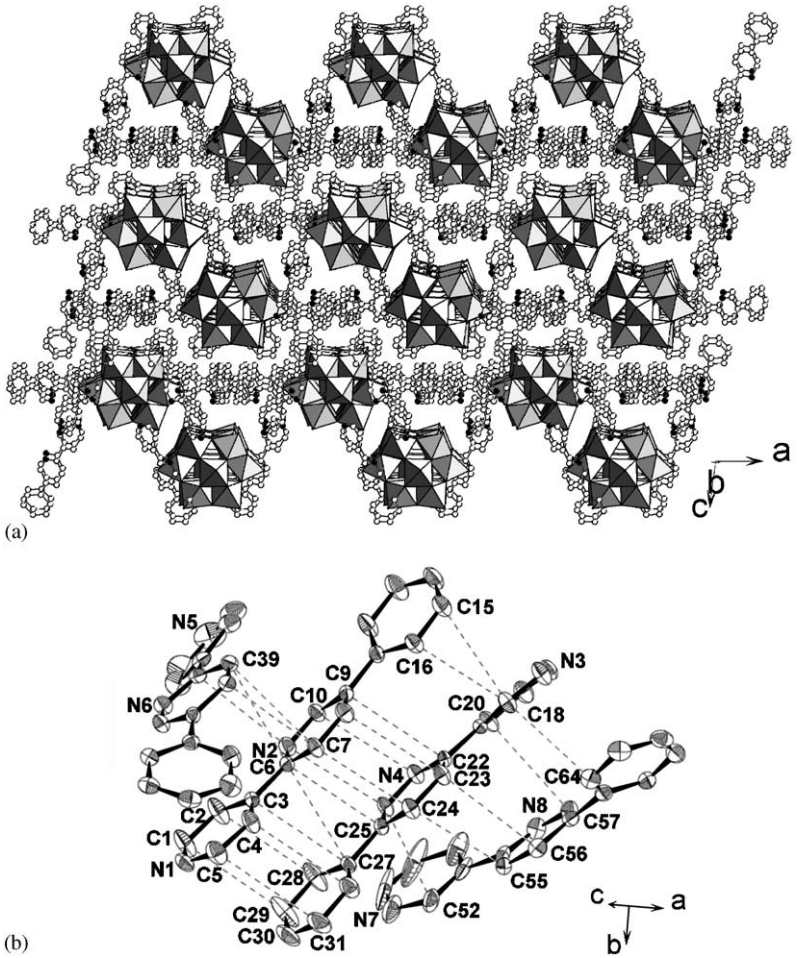


Fig. 3. (a) A view of the packing structure along the *b* axis illustrating the compact packing of pbpys to accommodate one-dimensional inorganic double chains of $PMo_{12}O_{40}^{3-}$ clusters. (b) Packing map of organic molecules (π–π interaction distances: 3.503–3.888 Å).

The peaks appear at 1090, 962, 912 and 804 $cm^{-1}$ attributed to *v*(P–O), *v*(Mo–$O_d$), *v*(Mo–$O_b$–Mo) and *v*(Mo–$O_c$–Mo) ($O_d$ = terminal oxygen, $O_b$ = bridged oxygen of two octahedral sharing a corner, $O_c$ = bridged oxygen of two octahedral sharing an edge), respectively. The peaks at 1462, 1516, 1643 and

1689 $cm^{-1}$ are attributed to characteristic vibrations of pbpy.

The UV spectrum of compound **1** measured in DMF solution is similar to that of free α-$H_3PMo_{12}O_{40}$ in the same solution (Fig. 6). Only one absorption peak, appearing at 298 nm in the UV region was observed in the UV spectrum of **1**, which is assigned to the charge-transfer absorption band of terminal and bridging oxygen atoms to metal atoms. This suggests that compound **1** is entirely disruptive in dilute solution. This was also observed in previous papers too [17].

### 3.3. Voltammetric behavior

#### 3.3.1. Voltammetric behavior of *1*-CPE in aqueous electrolyte

As is known, $PMo_{12}O_{40}^{3-}$ anion is unstable in neutral and basic aqueous solution and undergoes a series of hydrolysis process but is fairly stable in acidic aqueous solution [18]; therefore, electrochemical studies of **1**-CPE were carried out in acidic aqueous solutions.

Fig. 7 presents the cyclic voltammograms for **1**-CPE in 1 M $H_2SO_4$ aqueous solution at different scan rates. It were clearly seen that in the potential range from +800 to −200 mV, three reversible redox peaks appeared and the peak potentials $E_{1/2} = (E_{pa} + E_{pc})/2$ were +347 (I), +191 (II), and −18 (III) mV (scan rate: 20 mV $s^{-1}$), respectively. Redox peaks I–I′, II–II′ and III–III′ should be ascribed to three consecutive two-electron processes of Mo, respectively. When the scan rate varied from 20 to 200 mV $s^{-1}$ (see Fig. 7), the peak potentials changed gradually: the cathodic peak potentials shifted toward the negative direction and the corresponding anodic peak potentials to the positive direction with increasing scan rates. When scan rates were lower than 110 mV $s^{-1}$, the peak currents were proportional to the scan rate, which indicates that the redox process of **1**-CPE is surface-controlled, ideally reversible, and the exchanging rate of electrons is fast; however, when scan rates were higher than 110 mV $s^{-1}$, the peak currents were proportional to the square root of the scan rate, which indicates that the redox process of **1**-CPE is diffusion-controlled.

Table 2
Donor–acceptor interactions of compound **1**

| Interaction | Distance (Å) | Interaction | Distance (Å) |
|---|---|---|---|
| O(12)…N(1) | 2.881 | OW(1)…N(8) | 2.974 |
| O(35)…N(1) | 3.16 | OW(1)…OW(2) | 2.511 |
| O(6)…N(1) | 3.325 | OW(2)…C(37) | 2.863 |
| O(16)…N(1) | 2.991 | OW(2)…N(2) | 3.024 |
| O(10)…N(3) | 3 | OW(2)…OW(4) | 2.574 |
| O(22)…N(3) | 2.905 | OW(3)…OW(4) | 2.745 |
| O(24)…N(3) | 3.036 | OW(3)…N(4) | 2.997 |
| O(8)…N(3) | 2.889 | O(23)…C(33) | 3.046 |
| O(38)…N(5) | 2.947 | O(25)…C(53) | 3.125 |
| O(24)…N(7) | 2.698 | O(36)…C(2) | 3.113 |

The increase of peak-to-peak separation between the corresponding anodic and cathodic peaks with increasing scan rates may be explained as follows: (i) the reduction of compound **1** immobilized in the CPE is accompanied by the evolution of protons from solution to maintain charge neutrality. The encapsulation of **1** into a CPE may slow down the penetration rate of protons from solution into the particles and decrease the electron exchange rate to some extent. With increasing scan rate, the diffusion rate of the protons into the particles begins to determine the electrochemical reduction rate. (ii) The electron exchange rate between the insoluble solid **1** and the electrode may be slower than that between the soluble POM anion and electrode.

#### 3.3.2. pH-dependent electrochemical behavior of *1*-CPE

The pH of the supporting electrolyte has a slight effect on the electrochemical behavior of the **1**-CPE in $H_2SO_4 + Na_2SO_4$ aqueous solutions. As shown in

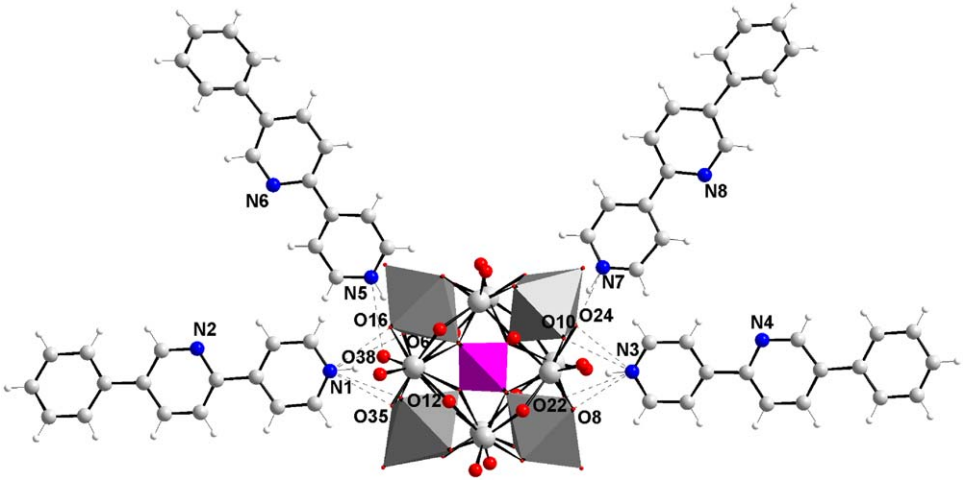


Fig. 4. A view showing the weak interaction of N…O occurring between organic cations and inorganic anion.

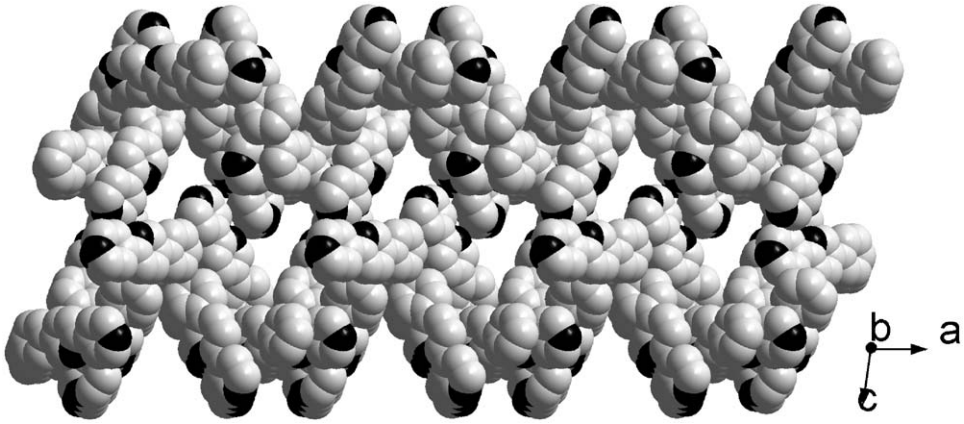


Fig. 5. Space-filling top view of organic cations showing the channels with polyoxometalate anions and water molecules omitted.

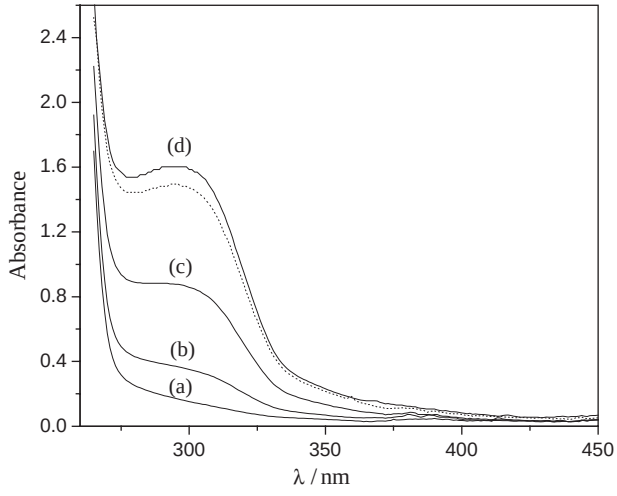


Fig. 6. The electronic spectra for **1** and free α-$H_3PMo_{12}O_{40}\cdot xH_2O$ in DMF. a, b, c and d represent different concentration of **1** in solution: 1, 2, 4 and $8\times10^{-4}$ M, respectively. The dot line represents the free α-$H_3PMo_{12}O_{40}\cdot xH_2O$ with a concentration of $10^{-4}$ M.

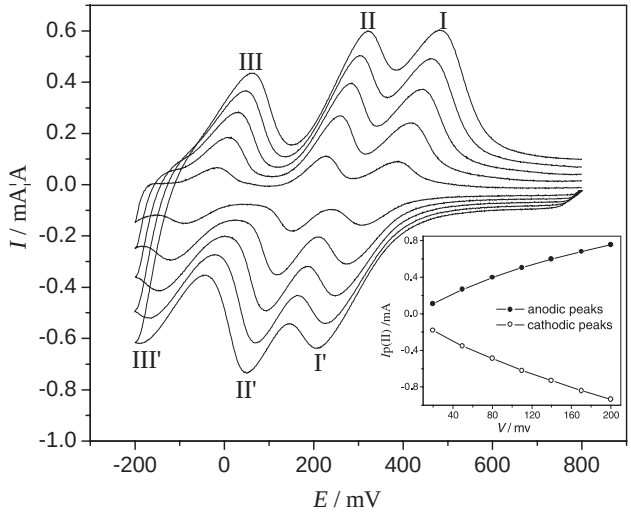


Fig. 7. The cyclic voltammograms of **1**-CPE in 1 M $H_2SO_4$ aqueous solution at different scan rates (from inner to outer: 20, 50, 80, 110 and 140 mV $s^{-1}$). The inset shows plots of the anodic and the cathodic peak II–II′ current against scan rates.

Fig. 8, it can be clearly seen that along with increasing pH, the anodic peaks potentials have no perceptible change whereas the corresponding cathodic potentials all gradually shift to the more negative potential direction, and both the anodic and cathodic peak currents decreased. Reduction of **1** in CPE is accompanied by the evolution of protons from solution to the wetted electroactive section of the electrode to maintain charge neutrality. Along with increasing pH, slower penetration of protons to the wetting section of the **1**-CPE should be the reason for the current decrease, and the more negative reduction potentials can be elucidated by the Nernst equation [19].

### 3.3.3. *Stability and surface-renewal of **1**-CPE*

In the experiment, **1**-CPE showed higher stability. When the scanning range was maintained from 800 to −200 mV, the electrodes were stable over 500 cycles at a scan rate 100 mV $s^{-1}$ and the current response remained almost unchanged. When the **1**-CPE was stored at room temperature (20–25 °C) for at least 3 months, the current response remained almost unchanged. The remarkable stability for **1**-CPE should be ascribed to the insolubility of the inorganic–organic hybrid POM material. The extensive hydrogen bonding and aryl packing interactions existed in crystal structure may serve the insolubility of **1** in aqueous solution. Compared with POM surface-modified electrodes fabricated by the conventional methods, the three-dimensional CPE have certain distinct advantages. One of the main attractions of the use of **1**-CPE is that squeezing a little carbon paste out of the tube can renew the bulk-modified CPE when needed. Experimental results demonstrated that 15 successively renewals did not result in an observable

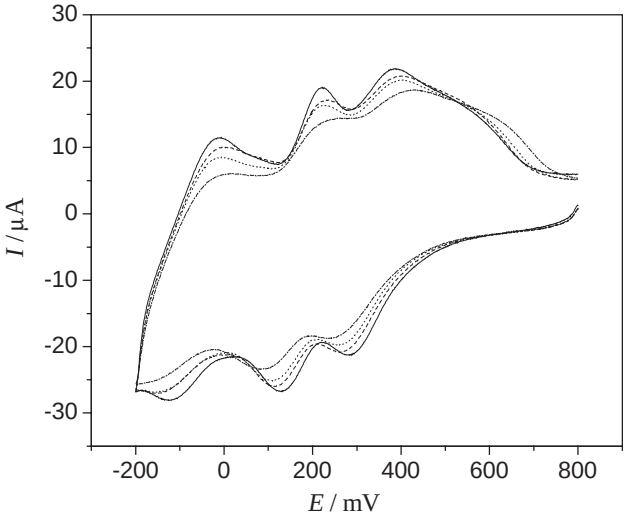


Fig. 8. The cyclic voltammograms for **1**-CPE in $H_2SO_4+Na_2SO_4$ aqueous solutions with different pH values (from outer to inner: 0.35, 0.48, 0.61 and 0.82). Scan rate: $50\,mV\,s^{-1}$.

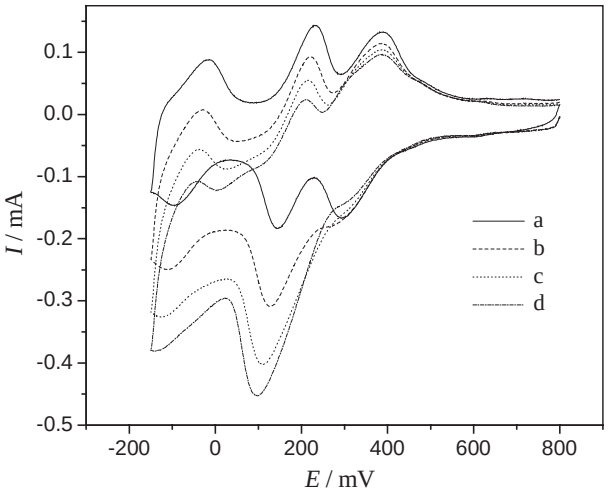


Fig. 9. Cyclic voltammograms of **1**-CPE in 1 M $H_2SO_4$ containing different concentrations of $NaClO_3$: (a) 0 mM, (b) 1.0 mM, (c) 5.0 mM and (d) 7.5 mM. Scan rate: $30\,mV\,s^{-1}$.

change of currents whereas it had a relative standard deviation of 5.8% for a gel film electrode [9(a)]. This is especially useful for electrocatalytic studies since catalytic activity decreases when the electrode bare surface is destroyed.

### 3.3.4. *Electrocatalytic activity of **1**-CPE*

As is known, POMs have been exploited extensively in electrocatalytic reductions [20]. For example, Dong et al. observed that $SiW_{12}O_{40}^{4-}$ could be used as an electrocatalyst for the reduction of nitrite [21]; Keita et al. observed that two-electron-reduced $SiMo_{12}O_{40}^{4-}$ could reduce nitrite in acidic solution [22]. Toth and Anson had applied the iron (III)-substituted Keggin-type POMs as catalysts for the reduction of hydrogen peroxide and nitrite [23]. Here, Compound **1** was employed to fabricate POM modified electrodes to electrocatalytic the reduction of chlorate, hydrogen peroxide and nitrite.

*3.3.4.1. Electrocatalytic activity of **1**-CPE for the reduction of chlorate.* Fig. 9 shows cyclic voltammograms for the electrocatalytic reduction of chlorate by **1**-CPE in 1 M $H_2SO_4$ aqueous solution. It can be seen clearly that with addition of chlorate, the catalytic wave appears mainly on the second and the third reduction waves (Peaks II and III) of **1**, corresponding to two- to four-electron and four- to six-electron reduction of $PMo_{12}O_{40}^{3-}$, respectively; peak I is almost unaffected, which is consistent with other POM-modified electrodes which have catalytic activity toward the reduction of bromate and hydrogen peroxide [9(a),12(a)]. We have noted that four-electron-reduced species have better catalytic activity than six-electron-reduced species for the electroreduction of chlorate.

*3.3.4.2. Electrocatalytic activity of **1**-CPE for the reduction of hydrogen peroxide.* Owing to high overpotential required at most electrode surfaces for direct electroreduction of hydrogen peroxide, no obvious response is observed for hydrogen peroxide on bare CPE in the range from +800 to −150 mV. Fig. 10 shows cyclic voltammograms for the electrocatalytic reduction of hydrogen peroxide by **1**-CPE in 0.5 M $H_2SO_4$ solution. Different from electrocatalytic reduction of chlorate, all three peaks exhibit catalytic activity for the reduction of hydrogen peroxide. Similarly, the four-electron-reduced species (peak II) have better catalytic activity than two- and six-electron-reduced species. Generally, low scan rates (such as 5, 10 or $20\,mV\,s^{-1}$) are used to obtain noticeable catalytic currents, however, a high scan rate ($50\,mV\,s^{-1}$) was used in the electrocatalytic reduction of hydrogen peroxide and catalytic currents also were observed clearly. This means that the reduction of hydrogen peroxide at **1**-CPE is fast.

*3.3.4.3. Electrocatalytic activity of **1**-CPE for the reduction of nitrite.* The catalytic reduction of nitrite on **1**-CPE can be seen clearly in Fig. 11, which shows cyclic voltammograms in 0.5 M $H_2SO_4$ solution. Unlike the electrocatalytic reduction of chlorate and hydrogen peroxide, the catalytic wave appears on the first and third reduction waves (peaks I and III): the cathodic currents rise while the anodic currents decease and disappear. Namely, two- and six-electron-reduced species exhibit good catalytic activity for the reduction of nitrite, while the four-electron-reduced species (peak II) have almost been affected.

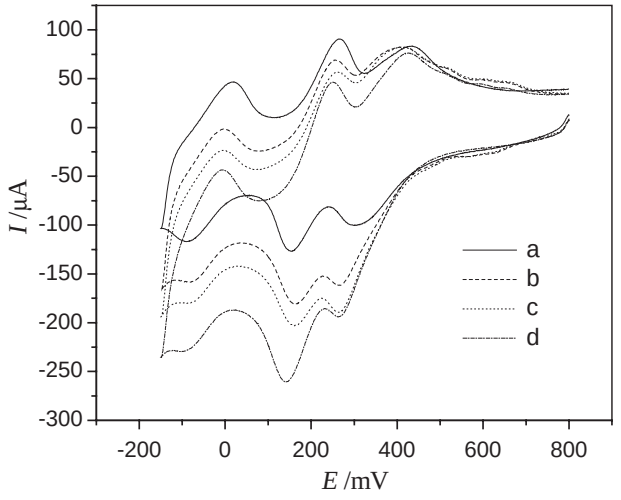


Fig. 10. Cyclic voltammograms of **1**-CPE in 0.5 M $H_2SO_4$ containing different concentrations of $H_2O_2$: (a) 0 mM, (b) 5.0 mM, (c) 10.0 mM and (d) 15.0 mM. Scan rate: 50 mV $s^{-1}$.

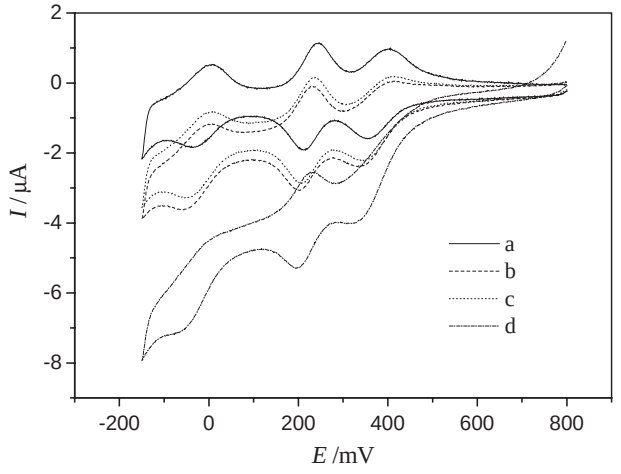


Fig. 11. Cyclic voltammograms of **1**-CPE in 0.5 M $H_2SO_4$ containing different concentrations of nitrite: (a) 0 mM, (b) 5.0 mM, (c) 7.5 mM and (d) 15.0 mM. Scan rate: 50 mV $s^{-1}$.

## 4. Conclusion

In this paper, the solid hybrid material **1** was prepared by hydrothermal reaction. In compound **1**, the anions extended its linkage into a one-dimensional inorganic double chain-like structure via weak interactions of O…O. The organic moiety exhibits regular packing with offset aromatic–aromatic interactions between the pbpys, leading to compact supramolecular framework structure to accommodate inorganic double chains. Hybrid **1** was employed to fabricate the POM modified electrodes to electrocatalytic reactions. The results indicate that the **1** retained Keggin molybdate anion electrocatalytic activities toward the reduction of chlorate, hydrogen peroxide and nitrite, which promise to compete well with traditional POM modified electrodes. Compared with the conventional POM-modified electrodes, **1**-CPE presents a good stability, which is especially important for practical applications. The stability of **1**-CPE may stem from the extensive hydrogen bonding and aryl packing interactions in compound **1**. It also indicates that organic pbpy with an extended π-electron conjugated system is a good candidate for assembling polyanion clusters to form stable hybrids which may further extend the application of POM in CME materials.

## Acknowledgment

This work was financially supported by the Natural Science Foundation of China (20271001).

## References

[1] (a) E. Coronado, J. Gómez-García, Chem. Rev. 98 (1998) 273–296;
(b) C.L. Hill, Chem. Rev. 98 (1998) 1–2;
(c) J.T. Rhuie, C.L. Hill, D.A. Judd, R.F. Schinazi, Chem. Rev. 98 (1998) 327–357;
(d) J.M. Lehn, Angew. Chem. 27 (1989) 89;
(e) E.B. Wang, C.W. Hu, L. Xu, Concise Polyoxometalates, Chemiscal Industry, Beijing, 1997.
[2] M.T. Pope, Heteropoly and Isopoly Oxometalates, Spriger, Berlin, 1983.
[3] M.T. Pope, A. Müller (Eds.), Polyoxometalte Chemistry, Kluwer, Dordrecht, 2001.
[4] (a) T. Yamase, Chem. Rev. 98 (1998) 307–325;
(b) L.C. Baker, D.C. Glick, Chem. Rev. 98 (1998) 3–49;
(c) M. Misono, Chem. Rev. 98 (1998) 199;
(d) D.E. Katsoulis, Chem. Rev. 98 (1998) 359–387.
[5] (a) P. Mialane, A. Dolbecq, L. Lisnard, A. Mallard, J. Marrot, F. Sécheresse, Angew. Chem. Int. Ed. 41 (2002) 2398–2401;
(b) C.D. Peloux, P. Mialane, A. Dolbecq, J. Marrot, F. Sécheresse, Angew. Chem. Int. Ed. 41 (2002) 2808–2810;
(c) E. Coronado, J.R. Galán-mascarós, C. Giménez-saiz, C.J. Gómez-garcía, C. Rovira, Judit Tarrés, Smail Triki, Jaume Veciana, J. Mater. Chem. 8 (1998) 313–317.
[6] (a) E. Coronado, C. Giménez-Saiz, C.J. Gómez-García, S.C. Capelli, Angew. Chem. Int. Ed. 43 (2004) 3022–3025;
(b) C.D. Peloux, A. Dolbecq, P. Barboux, G. Laurent, J. Marrot, F. Sécheresse, Chem. Eur. J. 10 (2004) 3026–3032;
(c) E. Coronado, J.R. Galán-Mascarós, C. Giménez-Saiz, C.J. Gómez-García, E. Martínez-Ferrero, M. Almeida, E.B. Lopes, Adv. Mater. 16 (2004) 324–327;
(d) C.J. Gomez-Garcia, C. Gimenez-saiz, S. Triki, E. Coronado, L. Ducasse, P. Le Magueres, L. Ouahab, P. Delhaes, Synth. Met. 70 (1995) 783;
(e) C.J. Gomez-Garcia, C. Gimenez-saiz, S. Triki, E. Coronado, P. Le Magueres, L. Ouahab, L. Ducasse, C. Sourisseau, P. Delhaes, Inorg. Chem. 34 (1995) 4139;
(f) C.J. Gomez-Garcia, L. Ouahab, C. Gimenez-saiz, S. Triki, E. Coronado, P. Delhaes, Angew. Chem., Int. Ed. 33 (1994) 223;
(g) E. Coronado, J.R. Galán-Mascarós, C. Giménez-Saiz, C.J. Gómez-García, E. Martínez-Ferrero, M. Almeida, E.B. Lopes, S.C. Capelli, R.M. Llusar, J. Mater. Chem. 14 (12) (2004) 1867–1872.

[7] (a) X. Xi, G. Wang, B. Liu, S. Dong, Electrochim. Acta 40 (1995) 1025;
(b) J.E. Toth, F.C. Anson, J. Am. Chem. Soc. 111 (1989) 2444;
(c) G. Bidan, E.M. Genies, M. Lapkowski, J. Electroanal. Chem. 251 (1988) 297;
(d) M. Sadakane, E. Steckhan, Chem. Rev. 98 (1998) 219.
[8] (a) D. Ingersoll, P.J. Kulesza, L.R. Faulkner, J. Electrochem. Soc. 141 (1994) 140;
(b) J.M. Zen, A.S. Kumar, D.M. Tsai, Electroanalysis 15 (2003) 1073;
(c) D. Martel, A. Kuhn, P.J. Kulesza, M.T. Galkowski, M.A. Malik, Electrochim. Acta 46 (2001) 4197–4204;
(d) D. Martel, A. Kuhn, Electrochim. Acta 45 (2000) 1829–1836;
(e) A. Kuhn, N. Mano, C. Vidal, J. Electrochem. Soc. 462 (1999) 187–194;
(f) S. Liu, Z. Tang, E. Wang, S. Dong, Thin Solid Film 339 (1997) 277.
[9] (a) P. Wang, Y. Yuan, Z.B. Han, G.Y. Zhu, J. Mater. Chem. 11 (2001) 549;
(b) W. Song, Y. Liu, N. Lu, H. Xu, C. Sun, Electrochim. Acta 45 (2000) 1639.
[10] (a) B. Keita, D. Bouaziz, L. Nadjo, J. Electroanal. Chem. 302 (1991) 47;
(b) A. Padadakis, A. Souliotis, E. Papaconstantinou, J. Electroanal. Chem. 435 (1997) 17;
(c) A.M. Bond, J.B. Cooper, F. Marken, D.M. Way, J. Electroanal. Chem. 396 (1995) 407.
[11] (a) P. Wang, X. Wang, G. Zhu, Electrochim. Acta 46 (2000) 637;
(b) P. Wang, X. Wang, L. Bi, G. Zhu, Analyst 125 (2000) 1291.
[12] (a) X.L. Wang, Z.H. Kang, E.B. Wang, C.W. Hu, Chem. Lett. (2000) 1030;
(b) X.L. Wang, Z.H. Kang, E.B. Wang, C.W. Hu, Mater. Lett. 56 (2002) 393;
(c) X.L. Wang, H. Zhang, E.B. Wang, C.W. Hu, Mater. Lett. 58 (2004) 1661;
(d) X.L. Wang, Q. Zhang, Z.B. Han, E.B. Wang, Y.Q. Guo, C.W. Hu, J. Electroanal. Chem. 563 (2004) 221.
[13] (a) K. Kalcber, Electroanalysis 2 (1990) 419;
(b) X.L. Wang, E.B. Wang, Y. Lan, C.W. Hu, Electroanalysis 14 (2002) 1116;
(c) X.L. Wang, Z.B. Han, E.B. Wang, H. Zhang, C.W. Hu, Electroanalysis 15 (2003) 1460.
[14] (a) G.M. Sheldrick, SHELXS 97: Programs for Crystal Structure Solution, University of Göttingen, Germany, 1997;
(b) G.M. Sheldrick, SHELXL 97: Programs for Crystal Structure Refinement, University of Göttingen, Germany, 1997.
[15] A.-S.J. Wery, J.-M. Gutierrez-Zorrilla, A. Luque, P. Vitoria, P. Roman, M. Martinez-Ripoll, Polyhedron 17 (1998) 1247.
[16] Z.G. Han, Y.L. Zhao, J. Peng, H.Y. Ma, Q. Liu, E.B. Wang, N.H. Hu, J. Solid State Chem. 177 (11) (2004) 4325–4331.
[17] (a) J.-Y. Niu, X.-Z. You, C.-Y. Duan, H.-K. Fun, Z.-Y. Zhou, Inorg. Chem. 35 (1996) 4221;
(b) J.-Y. Niu, Q. Wu, J.-P. Wang, J. Chem. Soc. Dalton Trans. 1 (2002) 2512.
[18] (a) C. Rocchiccioli-Deltcheff, M. Fournier, R. Franck, R. Thouvenot, Inorg. Chem. 22 (1983) 207;
(b) C. Sanchez, J. Livage, J.P. Launay, M. Fournier, Y. Jeannin, J. Am. Chem. Soc. 105 (1982) 3194.
[19] (a) J. Wang, Analytical Electrochemistry, VCH, New York, 1994;
(b) C.M.A. Brett, A.M.O. Brett, Electrochemistry Principles, Methods and Applications, Oxford University Press, Oxford, 1993 Chapter. 2.
[20] E. Papaconstantinou, A. Ioannidis, A. Hiskia, P. Argitis, D. Dimoticali, S. Korres, M. T. Pope and A. Müller (Eds.), Polyoxometalates: from Platonic Solids to Antiretroviral Activity, Kluwer, Dordrecht, 1993, p. 327; Mol. Eng. 3 (1993) 263.
[21] S. Dong, X. Xi, M. Tian, J. Electroanal. Chem. 385 (1995) 227.
[22] B. Keita, A. Belhouari, L. Nadjo, R. Contant, J. Electroanal. Chem. 381 (1995) 243.
[23] J.E. Toth, F.C. Anson, J. Electroanal. Chem. 256 (1988) 361.